Int Nano Lett (2017) 7:123–131
DOI 10.1007/s40089-017-0205-3

ORIGINAL ARTICLE

Green synthesis of manganese oxide nanoparticles for the electrochemical sensing of *p*-nitrophenol

Vineet Kumar[1,2] · Kulvinder Singh[1] · Shaily Panwar[1] · Surinder Kumar Mehta[1]

Received: 8 May 2016 / Accepted: 23 February 2017 / Published online: 27 March 2017

Abstract Manganese oxide (MnO) NPs are widely used in contaminant sensing, drug delivery, data storage, catalysis and biomedical imaging. Green synthesis of NPs is important due to increased concern of environmental pollution. Green chemistry based synthesis of NPs is preferred due to its ecofriendly nature. In this study, MnO NPs of different sizes were synthesized in aqueous medium using clove, i.e., *Syzygium aromaticum* extract (CE) as reducing and stabilizing agents. These NPs were used for the electrochemical sensing of *p*-nitrophenol (PNP). The synthesis of MnO NPs was over in 30 min. MnO NPs of different sizes were obtained by varying metal ion concentration, metal ion volume ratio, CE concentration, CE volume ratio, and incubation temperature. Selectively, ~4 nm MnO NPs were used for electrochemical sensing of paranitrophenol. The MnO NPs modified gold electrodes detected PNP with good sensitivity, 0.16 μA μM^{-1} cm^2. The limit of PNP detection was 15.65 μM. The MnO NPs prepared using CE based green chemistry approach is useful for PNP sensing. These NPs can also be useful for various in vivo applications in which the NPs come in human contact.

Keywords Manganese oxide nanoparticles · *p*-Nitrophenol · Electrochemical sensor · Clove · *Syzygium aromaticum* · Plant extract

Introduction

p-Nitrophenol is a toxic pollutant released from textile industry, leather industry, iron and steel manufacturing, foundries, pharmaceutical manufacturing, rubber processing, and electrical and electronic components production industry [1]. PNP is also released from diesel exhaust particles and as a degradation product of the insecticides [2, 3]. Hence, PNP contaminates water and environment. Acute short-term inhalation and/or ingestion of PNP in humans leads to headache, drowsiness, nausea, and cyanosis, i.e., blue color in lips, ears and fingernails [4]. PNP is also considered as non-genotoxic drug impurity. According to US Environment Protection Agency, US Food and Drug Administration draft and European Medicines Agency guidelines, non-genotoxic impurities can be used in amounts less than 4 mg day^{-1}. But there is no exact threshold limit for PNP usage, and maximum usable limit has to be determined on case-to-case basis [5]. Recent studies have documented toxic effect of PNP on animals. PNP has endocrine disrupting effect on Japanese quails. PNP exposure at even 10 μg kg^{-1} body weight caused hypothalamic pituitary gonadal toxicity. Hence, PNP can also hinder the reproductive processes of animals. Similar endocrine disrupting effect of PNP was observed in rats [2, 6, 7]. Newborn rats were found to experience more

Kulvinder Singh and Shaily Panwar contributed equally to this work.

Electronic supplementary material The online version of this article (doi:10.1007/s40089-017-0205-3) contains supplementary material, which is available to authorized users.

✉ Vineet Kumar
vineetkumar22@gmail.com

✉ Surinder Kumar Mehta
skmehta@pu.ac.in

[1] Department of Chemistry and Centre for Advanced Studies in Chemistry, Panjab University, Sector 14, Chandigarh, UT 160014, India

[2] Present Address: Department of Biotechnology, School of Life Sciences, DAV University, Sarmastpur, NH-44, Jalandhar, Punjab 144012, India

toxic effect of PNP than young rats [8]. PNP also has toxic effect on soil microalgae and cyanobacteria [9].

So, there is a need to detect PNP with good sensitivity. Electrochemical sensors have been reported for the detection of PNP. NPs use has been reported to increase the sensitivity of PNP detection system. Most of these studies have used NPs obtained by means of chemical synthesis. Chemical syntheses of NPs involve chemicals which can impart toxicity to NPs [10–15]. Toxicity of NPs has been directly linked to the use of chemicals as reducing and capping agents [16–18]. Some studies have used less toxic chemical reducing agents, but these studies have used acidic or basic environment for the MnO_2 NPs synthesis. Further, the MnO_2 NPs obtained are bigger in size [19, 20]. Balan et al. have prepared MnO_2 NPs without the use of any surfactant. These NPs may aggregate on long time storage and may impart toxicity as the bare surface is more reactive. Thus, these NPs can be toxic to environment and living organisms [21, 22]. So, the greener route of NPs synthesis is preferred. Green chemistry is a recent branch in chemistry and focuses on minimum or no use of harmful chemicals. In context to NPs synthesis, it involves minimum use of organic solvents as reaction medium and/or replacing it with water or less toxic solvents and use of greener reducing and/or stabilizing agents [18, 23]. Hence, green chemistry approach offers minimum toxic products and by- products. In present study, CE was used as reducing and capping agent for the synthesis of stable MnO NPs in water. To best of our knowledge this is the first report on plant extract use preparing MnO NPs for electrochemical sensing of PNP (Scheme 1).

Experimental

Materials

Manganese (II) acetate tetrahydrate, butyl carbitol acetate (BCA), PNP and other chemicals used in the study were of analytical grade and were purchased from Merck and Aldrich. Dry clove (*Syzygium aromaticum* L.) flower buds were purchased from local grocery store.

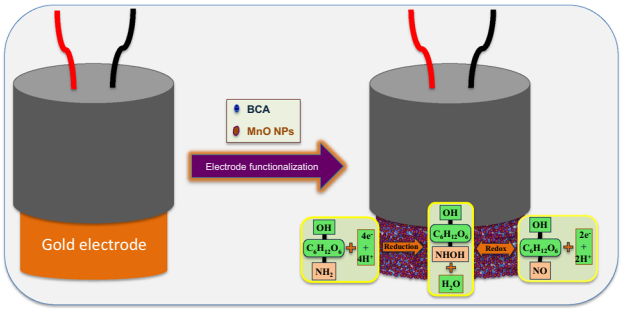

Scheme 1 Schematic representation of gold electrode modification with MnO NPs and electrochemical sensing

CE preparation and synthesis of MnO NPs

2 g powdered clove was put in flask containing 50 ml of DDW and boiled for 2 min. The mixture was cooled and centrifuged at 7500 rpm for 10 min. The clear supernatant was labelled as CE and was stored at 4 °C. To prepare MnO NPs, 40 mM metal ion, i.e., the aqueous solution of manganese acetate (II) tetrahydrate was mixed with 1 ml CE. The reaction mixture was incubated at room temperature, i.e., 25 °C.

To obtain MnO NPs of different sizes, physiochemical factors namely, metal ion concentration, clove extract (CE) concentration, metal ion volume, CE volume and incubation temperature were varied. Metal ion concentration was varied from 1 to 80 mM. 1 ml of varying metal ion concentration was incubated with 1 ml CE at room temperature (Supplementary table ST1†). The CE concentration was varied from 0.25 to 1 ml (Supplementary table ST2†). The effect of metal ion volume ratio on MnO NPs quantity and size was evaluated by varying metal ion volume from 1 to 5 ml (Supplementary table ST3†). CE volume was varied from 1 to 4 ml. Different volumes of CE were used for the MnO NPs synthesis while keeping metal ion volume 1 ml (Supplementary Table S4†). To see the effect of incubation temperature, 1 ml of 40 mM metal ion was incubated with 1 ml CE at different temperatures ranging from 25 to 85 °C (Supplementary table ST5†).

Characterization of MnO NPs

Reaction mixtures were screened for MnO NPs synthesis using UV–Visible spectroscopy. Reaction mixtures were diluted and 2 ml of diluted sample was subjected to UV–Visible spectroscopic analysis (JASCO V-530 UV–Visible spectrophotometer). UV–Visible spectra of MnO NPs prepared using 1 ml 40 mM metal ion and 1 ml CE at 25 °C were recorded at fix time interval, 0 (just after mixing), 15, 30, 60 and 120 min, respectively. Similarly, MnO NPs obtained by varying physiochemical factors were characterized at 30 min of reaction using UV–Visible spectroscopy.

The MnO NPs were characterized for size using dynamic light scattering technique. After 30 min of incubation, the reaction mixtures were centrifuged at 7000 rpm for 10 min to isolate MnO NPs. The pellets were redispersed in double distilled water (DDW) and centrifuged again to purify MnO NPs. So, purified MnO NPs were diluted 10–20 times and were analyzed directly for size using dynamic light scattering technique (DLS, Malvern Nano-S90 zetasizer nanoseries). The size and morphology

of the NPs was further characterized by field emission scanning electron microscope (FESEM, Hitachi, Sv8010, 15 kv) and transmission electron microscope (TEM, Hitachi, H-7500, 120 kV).

X-ray diffraction (XRD, Panalytical D/Max-2500) analysis was performed to check the size and structural properties of MnO NPs. Infrared spectra were recorded with a fourier transform infrared (FTIR, Perkin Elmer Spectrum 400) spectrometer. Thermal analysis of MnO NPs and CE was carried out using thermal gravimetric analysis (TGA, SDT Q600 thermal analysis). The analysis was carried out at 20–1000 °C in nitrogen gas atmosphere.

Fabrication of MnO NPs based electrochemical sensor

Clean gold electrode (surface area = 3.014 mm^2) was polished with alumina slurry. The polished gold electrode was sonicated in DDW and dried thereafter. BCA and powdered MnO were mixed in 20: 80 ratio, respectively, to make slurry. The gold electrode was modified with MnO NPs slurry. The MnO NPs were coated on electrode surface so that MnO slurry cover entire electrode surface. The electrode was dried completely at 60 °C and used as so for electrochemical experiments. All the electrochemical sensing experiments were performed at room temperature using cyclic voltammeter (μAuto lab Type-III) with three-electrode configuration. Ag/AgCl with saturated KCl was used as a reference electrode. Pt wire was used as a counter electrode and the MnO NPs/BCA/gold electrode was used as working electrode. For all the measurements, 0.1 M phosphate buffer solution (pH 7.0) was used and all the solutions were prepared using DDW unless specified.

Electrochemical sensing of PNP

For electrochemical sensing of PNP, three different electrochemical techniques, namely, normal cyclic voltammetry (CV), differential pulse voltammetry (DPV), and amperometry were used. CV analysis of PNP was performed at 100 mV s^{-1} scan rate in aqueous medium, i.e., phosphate buffer using MnO NPs/BCA/gold electrode. Further, to check the mechanism behind PNP electrochemical response, CV measurements were conducted at 50–800 mV s^{-1} scan rate. Sensitivity and detection limit of MnO NPs/BCA/gold electrode were carried out using DPV technique. 200–550 μM PNP was tested over −0.3 to −0.9 voltage. To check the effect of interfering entity on the selectivity of MnO NPs/BCA/gold electrode, amperometric studies were conducted at fixed potential, −0.69 V. After constant time interval of 100 s, PNP and interfering compounds were introduced to the sensor system. First of all, 100 s after the scan, 0.1 ml of 1 mM PNP was added. Subsequently, K^+, Ni^{2+}, para-nitrobenzene, Mg^{2+}, cd^{2+}, oxamide, ortho-benzaldehyde, Hg^{2+} and nitromethane were introduced at 100 s interval. Further, to verify whether system remain active after interacting with interfering compounds, 0.1 ml of 1 mM PNP was added after 1100 and 1200 s to examine whether R2 is irreversible or not; Tafel equation was used (Eq. 1).

$$E_p = (b/2)\log v + \text{constant} \quad (1)$$

where Ep is the peak potential, b is the Tafel slope, and v is the scan rate. Tafel slope was calculated using Eq. (1) [24].

The transfer coefficient (α) was calculated using Eq. (2) [25]

$$b = \frac{2.303RT}{\alpha F} \quad (2)$$

R, T and F represent gas constant, temperature in Kelvin and Faraday constant, respectively. The value of αnα was calculated from the irreversible reduction of PNP, i.e., R2 using modified electrode according to the given Eq. (3) [24].

$$\alpha n_\alpha = \frac{0.048}{E_p - E_{p/2}} \quad (3)$$

Here, Ep is the peak potential and corresponds to ip, and Ep/2 is half height potential. Further, the total number of electrons for totally irreversible reaction R2 was calculated using Nicholson and Shain equation [26].

$$I_p = \left(2.99 \times 10^5\right) n\,(\alpha n_\alpha)^{1/2} \mathrm{ACD}^{1/2} v^{1/2} \quad (4)$$

Where n is the number of electrons, C is the concentration in mole cm^{-3}, D is the diffusion coefficient in cm^2 s^{-1} and A is the area in cm^2.

Randles–Sevcik equation, i.e., Eq. (5) was used to calculate the number of electron involved in this redox process.

$$I_\mathrm{p} = \left(2.69 \times 10^5\right) n^{3/2} \mathrm{ACD}^{1/2} v^{1/2} \quad (5)$$

Results and discussion

UV–Visible and morphological characterization of MnO NPs

NPs have absorption characteristics in the UV–Visible region [27]. The UV–Visible absorption intensity of NPs generally increases with an increase in NPs concentration [28]. In the present study, MnO NPs showed characteristic absorption peak at around 260–270 nm. The color of aqueous metal ion solution is transparent. On addition of CE the color of metal ion solution changed to reddish dark brown from transparent. This change in color of metal ion solution acts as visible indicator of MnO NPs synthesis (Supplementary figure S1a and 1b†). Time study of MnO

NPs reaction mixture at these reaction condition revealed that most of the MnO NPs synthesis was over in 30 min and further reaction did not led to an increase in MnO NPs synthesis (Supplementary figure S2a†). The DLS size of MnO NPs obtained at 30 min of reaction was 352 ± 11.493 nm (Supplementary figure S2b). With an increase in metal ion concentration from 1 to 10 mM, there was an increase in characteristic UV–Visible absorption intensity of MnO NPs. Further increase in metal ion concentration up to 40 mM has no effect on the UV–Visible absorption intensity (Supplementary figure S3a†). The peak intensity decreased with further increase in the metal ion up to 60 and 80 mM. This decrease in peak intensity may be due to the formation of bigger NPs as a result of aggregation of small NPs [29]. The size of NPs did not change much from 1 mM (365.61 ± 42.12 nm) to 40 mM (352.06 ± 11.493 nm) metal ion concentration (Supplementary table ST1†). However, the size of NPs steadily increased with subsequent increase in metal ion concentration up to 80 mM (1012.53 ± 53.23 nm). Further as the UV–Visible absorption at 10-40 mM was almost the same, the amount of MnO NPs recovered by centrifugation was more in case of 40 mM metal ion. Therefore, 40 mM metal ion concentration was used for further experiments. As the CE concentration decreased from 1 ml to 0.25 ml, there was a decrease in the UV–Visible absorption intensity (Supplementary figure S3b†). The size of NPs increased with an decrease in CE concentration up to 0.25 ml (Supplementary Table ST2†). The decrease in the intensity and increase in size of MnO NPs may be due to formation of fewer amounts of bigger MnO NPs in the deficiency of reducing and capping agents [28]. Therefore, 1: 1 volume ratio was better among other CE concentrations. However, as the metal ion volume increased from 1: 1 to 5: 1 (metal ion: CE) there was a decrease in the UV–Visible absorption intensity (Supplementary figure S3c†). This may be due to more dilution of CE and reaction mixture. Mixing metal ion and CE in appropriate concentration is necessary for the formation of stable small size NPs [30]. The decrease in the peak intensity may be due to the reaction of inappropriate proportion of metal ion and CE. This might have led to formation of fewer and bigger NPs due to destabilization of small NPs [31–33]. The size of NPs increased with increasing metal ion ratio from 352.06 ± 11.49 nm at 1: 1 to 1435 ± 96.38 nm at 5: 1 ratio (Supplementary table S3†).

Besides, as the CE volume ratio varied from 1: 1 to 1: 4 (metal ion: CE), there was a constant increase in the UV–Visible absorption intensity up to 1: 3 ratio (Supplementary figure S3d†). Subsequently, there was only a slight increase in the absorption intensity at 1: 4 ratio. Since the size of MnO NPs increased with increasing CE ratio, 1: 1 volume ratio was preferred over other volume ratios (Supplementary table ST4†). There was only a slight increase in the UV–Visible absorption intensity with an increase in incubation temperature from room temperature to 40 °C. However, the UV–Visible intensity decreased simultaneously with increasing incubation temperature up to 85 °C (Supplementary figure S3e†). The size of NPs increased with increasing incubation temperature from 25 to 85 °C (Supplementary table ST5†), which was in agreement with earlier studies [27, 28, 30]. 40 mM metal ion and 1: 1 metal ion to CE volume ratio was found to be appropriate condition for the synthesis of smaller sized MnO NPs in good quantity (Supplementary figure S2b†). So, these MnO NPs were subjected to detailed and more accurate morphology characterization using FESEM and TEM. FESEM coupled energy dispersive X-ray (EDX) detector was used for elemental analysis of MnO NPs. Mn and O peaks in the EDX spectrum of NPs confirmed that the NPs characterized using FESEM were of manganese chemical composition (Fig. 1a). FESEM analysis revealed that the average size of MnO NPs was 3.5 ± 1.88 nm (Fig. 1b and c).

The TEM analysis shows that MnO NPs were 2.5 ± 0.88 nm in size (Fig. 2a and b). XRD size was calculated using Scherer equation and was found to be 1.8 nm (Fig. 3a). The peak was collectively broad due to amorphous nature of biosurfactant moieties covering MnO NPs and small size of MnO NPs. The size of NPs obtained from FESEM and TEM analysis is more accurate than the size calculated using XRD [34]. Overall, MnO NPs were of approximately 4 nm average size.

Thermal gravimetric analysis also supports the XRD interpretation that MnO were surrounded by various CE moieties (Fig. 3b and c). Two sharp peaks were observed at ~68 °C and ~272 °C. As the MnO has degradation temperature more than 1700 °C, the noticed peaks could have been due to degradation of stabilizing moieties around MnO NPs [35].

Clove extract acts as reducing and stabilizing agent during the MnO NPs synthesis. So, the surface of MnO NPs is surrounded by various organic stabilizing moieties. Careful interpretation of various peaks in the FTIR spectrum of MnO NPs gave an idea of stabilizing moieties (Supplementary figure S4a†). FTIR peaks around 504, 554, 758 and 827 cm^{-1} were due to MnO NPs [36–40]. However, peaks around 603 (R-CH group), 922 (–C–O bond), 1220 (CH_2 group or C–O stretching), 1319, 1368 (C–O vibrations), 1475 (bending frequency methylene group), 1618 (aromatic C = C bond stretching), 1707 (C = O stretching vibrations), 2925 (–C = C bond) and 3393 (OH bond) cm^{-1} were observed mainly due to the presence of eugenol, caryophyllene, humulene and eugenol acetate in CE [41–43]. FTIR characterization of CE revealed similar peaks around 551, 600, 918, 1226, 1368, 1447, 1615, 1729, and 2936 cm^{-1} which were due to presence of these moieties (Supplementary figure S4b†). So, eugenol,

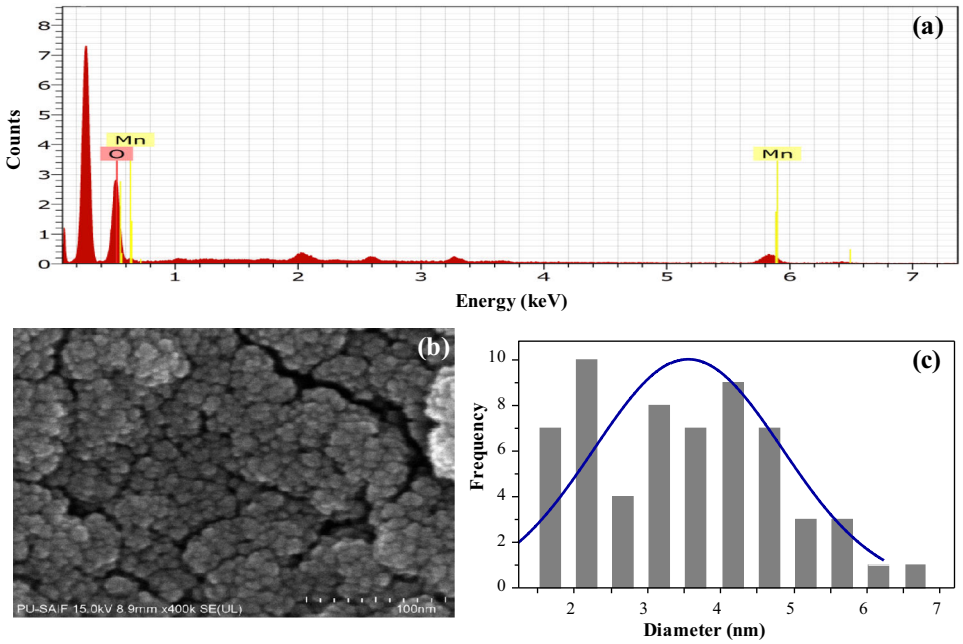

Fig. 1 FESEM characterization of MnO NPs prepared using CE. **a** EDX spectrum of MnO NPs showing Mn and O peaks, **b** FESEM image of MnO NPs, and **c** size distribution pattern of MnO NPs

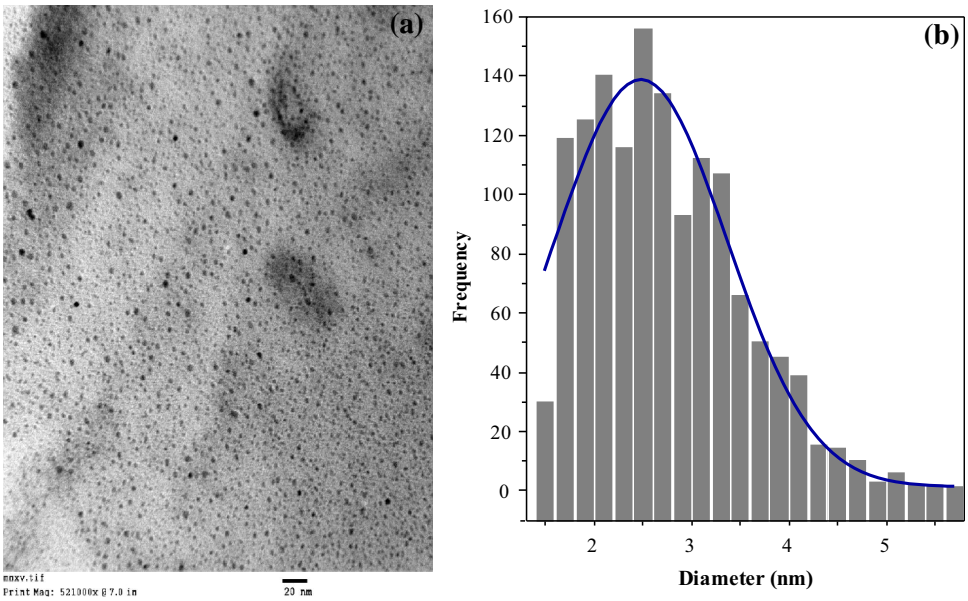

Fig. 2 TEM characterization of MnO NPs. **a** TEM image of MnO NPs, and **b** size distribution pattern of MnO NPs

caryophyllene, humulene and eugenol acetate moieties were mainly responsible for MnO NPs synthesis.

Electrochemical sensing of paranitrophenol using MnO NPs modified gold electrode

In CV, the electroactive surface of electrode induces oxidation and/or reduction of test sample. The oxidation and reduction process can be easily monitored by the oxidation or reduction peak in cyclic voltagram. CV analysis of test medium, i.e., phosphate buffer using MnO NPs/BCA/gold electrode did not show any oxidation or reduction peak. However, addition of 1 mM PNP to phosphate buffer induced the electrochemical response (Fig. 4a). A pair of reversible PNP reduction ($R1$) and oxidation ($O1$) peak was observed at 0.04 and 0.12 V, respectively, while an irreversible reduction peak ($R2$) was noticed at −0.69 V. So, PNP undergoes three step electrochemical responses on MnO NPs/BCA/gold electrode surface. The detailed mechanism of these responses was studied by varying the scan rate. Scan rate analysis revealed that the current response increases with an increase in scan rate in both the reduction and the redox process (Fig. 4b). Data analysis for finding rate determining step of $R2$ was carried out using

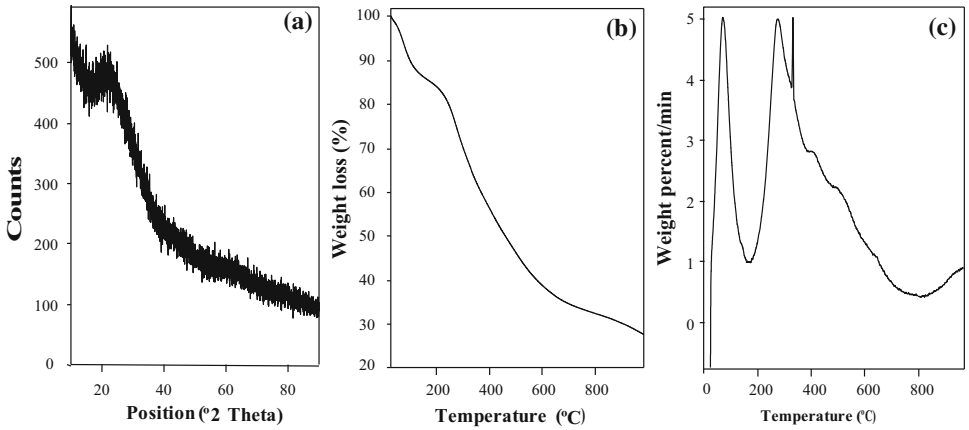

Fig. 3 **a** XRD spectrum of MnO NPs. *Broad peak* indicates that the MnO NPs are small in size and covered by biological moieties from CE, **b** TGA curve of MnO NPs, and **c** differential TGA curve. Peaks at ~68 and ~272 °C indicate degradation of surface covering CE stabilizer moieties as the degradation temperature of bulk MnO is above 1700 °C

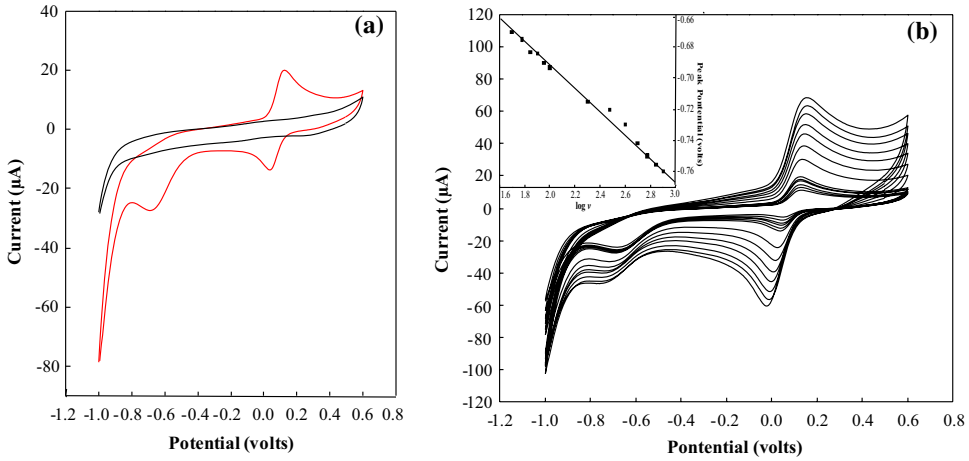

Fig. 4 CVs analysis of PNP using MnO NPs modified electrode. **a** Graph showing CV response of modified electrode in absence (*black line*) and presence (*red line*) of PNP. *Black line* represents response of MnO NPs/BCA/gold electrode to 0.1 M phosphate buffer (pH 7.0) and *red line* represents the electrochemical response of MnO NPs/BCA/gold electrode to PNP, and **b** cyclic voltammograms showing response of 1 mM PNP in PBS using MnO NPs/BCA/gold electrode at 50–800 mVs-1 scan rates. *Inset* Tafel plot on irreversible reduction reaction, i.e., peak current vs scan rate

Tafel equation, i.e., Eq. (1) [24]. *E*p versus log υ plot revealed that that *E*p increased linearly with an increase in log υ value. This indicated that the *R*2 process was irreversible (Fig. 4b Inset). The value of Tafel slope b as calculated from slope of Fig. 4b was found to be 0.144 V. This value of b indicated that only one electron was involved in the rate determining step of *R*2 [44].

The value of α, i.e., transfer coefficient as calculated for R2 using Eq. (2) was found to be 0.41 [25]. The value of αnα was calculated using Eq. 3 [24]. The αnα value for R2 process was 1.2. Furthermore, Nicholson and Shain equation, i.e., Eq. (4) was applied to calculate the total number of electrons involved in R2. Totally, four electrons were found to be involved in totally irreversible reaction R2 (Fig. 5a) [26]. However, to study the mechanism of redox peak formation, the effect of square root of scan rate on the redox peak, i.e., reversible peak (R1 and O1) was analyzed (Fig. 5b). Careful analysis using Randles–Sevcik equation (Eq. 5) revealed that two electrons were involved in the reversible redox process R1 and O1. Thus, the reversible reaction undergoes two-electron exchange process [45].

It is clear from above discussion that the irreversible reaction of PNP undergoes four electron gains, while the reversible reaction is a two-electron redox process. Our results are in agreement with previously documented studies [10, 15, 46]. PNP first undergoes irreversible reduction to form 4-(hydroxyamino) phenol. Then, it undergoes a pair of coupled redox, indicating the oxidation of 4-(hydroxyamino) phenol to 4-nitrosophenol, and its subsequent reversible reduction, respectively.

Sensitivity of the system

Differential pulse voltammetry technique was used to find out the exact sensitivity and detection limit of MnO NPs/BCA/gold electrode system for PNP (Fig. 6a and b). The

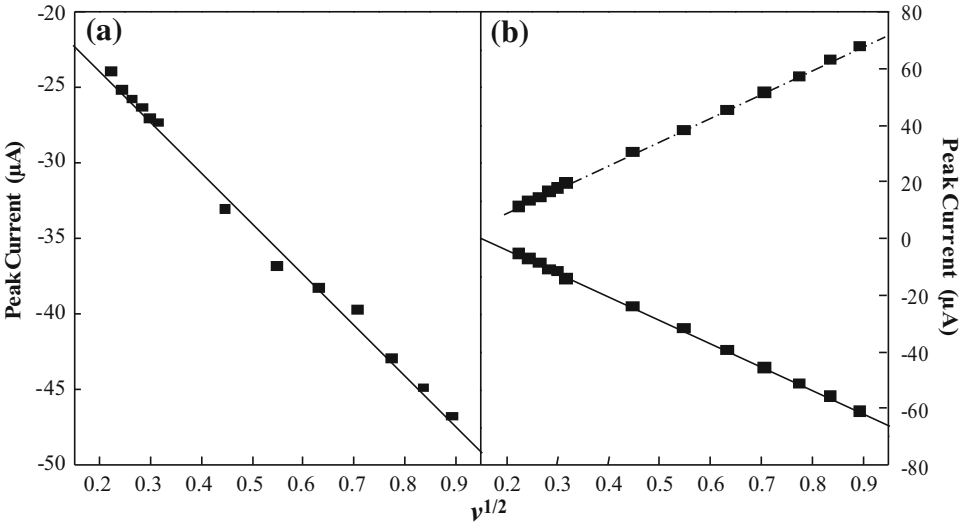

Fig. 5 Effect of square root of scan rate on peak current obtained using MnO NPs/BCA/gold electrode. **a** Effect of square root of scan rate on irreversible reduction peak current (R2), and **b** effect of square root of scan rate on reversible redox peak current (O1 *dotted line* and R1 *solid line*)

peak corresponding to reduction current increased linearly with increase in concentration of PNP. The sensitivity of the system was calculated using the following formula:

$$\text{Sensitivity} = \frac{\text{Slope of calibration curve}}{\text{Area of electrode}}$$

The sensitivity of the MnO NPs modified gold electrode system comes out to be 0.16 μA μM^{-1} cm^2. Furthermore, the detection limit was calculated using 3σ IUPAC criteria. The detection limit of PNP using DPV technique comes out to be 15.65 μM.

Selectivity and interference studies

The test sample may contain interfering substances along with PNP. The interference and selectivity of the MnO/BCA/gold electrode towards PNP detection system was analyzed by the amperometric studies. As the PNP was introduced to test medium, there was an increase in reductive current of the system (Fig. 7). As the interfering heavy metal ions and aromatic compounds were added, there was much less change in the current. This indicates that the present sensor did not recognize non-specific components. Interestingly, subsequent addition of PNP at 1100 and 1200 s has led to approximate constant increase in reductive current. This confirms that the current MnO NPs based sensing system is selective to PNP and can detect PNP in presence of various commonly present interfering substances like heavy metal ions and aromatic compounds.

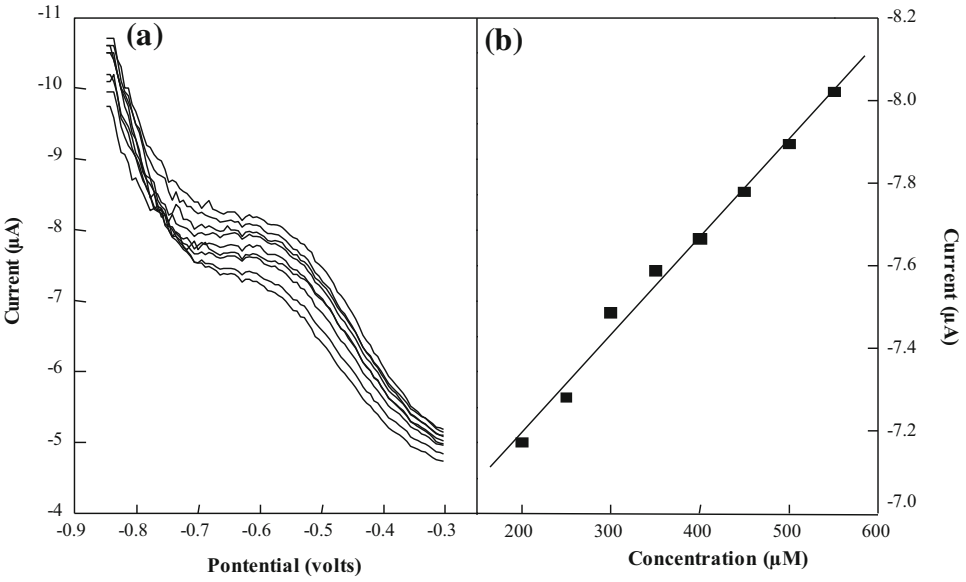

Fig. 6 **a** DPV plot showing effect of PNP concentration on the reduction current, and **b** calibration curve of PNP using DPV

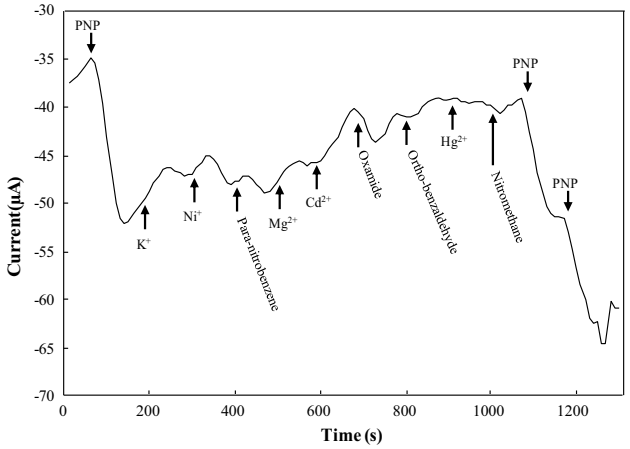

Fig. 7 Spectrum showing amperometric responses of MnO NPs/BCA/gold electrode to PNP in the presence of interfering compounds. This MnO NPs based sensor has good selectivity for PNP

Conclusions

MnO NPs of different sizes have been successfully synthesized using CE as reducing and stabilizing agent. MnO NPs fabricated using this green chemistry approach has been effectively used for the electrochemical detection of PNP. The MnO NPs/BCA/gold electrode has shown good electro catalytic activity to PNP. Hence, the as-prepared electrochemical sensor has good sensitivity and low limit of detection for PNP. The interference and selectivity studies revealed that the present system has good selectivity for PNP in presence of interfering moieties. So this MnO NPs based electrochemical sensor is a robust and sensitive technique for PNP detection. Further, the MnO NPs can also be very useful for sensing other harmful chemicals and in various in vivo biological applications.

Acknowledgements The authors are thankful to Central Instrumental Laboratory (CIL), Panjab University Chandigarh, India, for TEM, FESEM, and XRD measurements. VK is thankful to UGC for Dr. D. S. Kothari Postdoctoral Fellowship.

References

1. Podeh, M.R.H., Bhattacharya, S.K., Qu, M.: Effects of nitrophenols on acetate utilizing methanogenic systems. Water. Res. **29**, 391–399 (1995)
2. Li, X., Li, C., Suzuki, A.K., Taneda, S., Watanabe, G., Taya, K.: 4-Nitrophenol isolated from diesel exhaust particles disrupts regulation of reproductive hormones in immature male rats. Endocrine **36**, 98–102 (2009)
3. Ahmed, E., Nagaoka, K., Fayez, M., Abdel-Daim, M.M., Samir, H., Watanabe, G.: Suppressive effects of long-term exposure to *p*-nitrophenol on gonadal development, hormonal profile with disruption of tissue integrity, and activation of caspase-3 in male Japanese quail (*Coturnix japonica*). Environ. Sci. Pollut. Res. **22**, 10930–10942 (2015)
4. Mulchandani, C.M., Hangarter, Y., Lei, Y., Chen, W., Mulchandani, A.: Amperometric microbial biosensor for *p*-nitrophenol using *Moraxella* sp.-modified carbon paste electrode. Biosens. Bioelectron. **21**, 523–527 (2005)
5. Eichenbaum, G., Johnson, M., Kirkland, D., O'Neill, P., Stellar, S., Bielawne, J., DeWire, R., Areia, D., Bryant, S., Weiner, S., Desai-Krieger, D., Guzzie-Peck, P., Evans, D.C., Tonelli, A.: Assessment of the genotoxic and carcinogenic risks of *p*-nitrophenol when it is present as an impurity in a drug product. Regul. Toxicol. Pharm. **55**, 33–42 (2009)
6. Li, C., Taneda, S., Suzuki, A.K., Furuta, C., Watanabe, G., Taya, K.: Estrogenic and anti-androgenic activities of 4-nitrophenol in diesel exhaust particles. Toxicol. Appl. Pharm. **217**, 1–6 (2006)
7. Zhang, Y., Piao, Y., Li, Y., Song, M., Tang, P., Li, C.: 4-Nitrophenol induces Leydig cells hyperplasia, which may contribute to the differential modulation of the androgen receptor and estrogen receptor-α and -β expression in male rat testes. Toxicol. Lett. **223**, 228–235 (2013)
8. Koizumi, M., Yamamoto, Y., Ito, Y., Takano, M., Enami, T., Kamata, E., Hasegawa, R.: Comparative study of toxicity of 4-nitrophenol and 2, 4-dinitrophenol in newborn and young rats. J. Toxicol. Sci. **26**, 299–311 (2001)
9. Mallavarapu, M., Pearson, H.W., Kadiyala, V.: Toxicity of p-aminophenol and *p*-nitrophenol to Chlorella vulgaris and two species of Nostoc isolated from soil. Pestic. Biochem. Phys. **40**, 266–273 (1991)
10. Liu, Z., Dub, J., Qiu, C., Huang, L., Ma, H., Shen, D., Ding, Y.: Electrochemical sensor for detection of *p*-nitrophenol based on nanoporous gold. Electrochem. Commun. **11**, 1365–1368 (2009)
11. Lupu, S., Lete, C., Marin, M., Totir, N., Balaure, P.C.: Electrochemical sensors based on platinum electrodes modified with hybrid inorganic-organic coatings for determination of 4-nitrophenol and dopamine. Electrochim. Acta. **54**, 1932–1938 (2009)
12. Perreault, F., Popovic, R., Dewez, D.: Different toxicity mechanisms between bare and polymer-coated copper oxide nanoparticles in *Lemna gibba*. Environ. Pollut. **185**, 29–227 (2014)
13. Mhammedi, M.A.E., Achak, M., Bakasse, M., Chtaini, A.: Electrochemical determination of para-nitrophenol at apatite-modified carbon paste electrode: application in river water samples. J. Hazard. Mater. **163**, 323–328 (2009)
14. Li, J., Kuang, D., Feng, Y., Zhang, F., Xu, Z., Liu, M.: A graphene oxide-based electrochemical sensor for sensitive determination of 4-nitrophenol. J. Hazard. Mater. **201–202**, 250–259 (2012)
15. Singh, K., Kaur, A., Umar, A., Chaudhary, G.R., Singh, S., Mehta, S.K.: A comparison on the performance of zinc oxide and hematite nanoparticles for highly selective and sensitive detection of para-nitrophenol. J. Appl. Electrochem. **45**, 253–261 (2015)
16. Buzea, C., Blandino, I.I.P., Robbie, K.: Nanomaterials and nanoparticles: sources and toxicity. Biointerphases **2**, 17–71 (2007)
17. Kumar, V., Kumari, A., Guleria, P., Yadav, S.K.: Evaluating the toxicity of selected types of nanochemicals. Rev. Environ. Contam. Toxicol. **215**, 39–121 (2012)
18. Duan, H., Wan, D., Li, Y.: Green chemistry for nanoparticle synthesis. Chem. Soc. Rev. **44**, 5778–5792 (2015)

19. Balan, L., Ghimbeu, C.M., Vidala, L., Vix-Guterl, C.: Photoassisted synthesis of manganese oxide nanostructures using visible light at room temperature. Green. Chem. **15**, 2191–2199 (2013)
20. Dang, D., Cheney, M.A., Qian, S., Joo, S.W., Min, B.K.: A novel rapid one-step synthesis of manganese oxide nanoparticles at room temperature using poly(dimethylsiloxane). Ind. Eng. Chem. Res. **52**, 2750–2753 (2013)
21. Kumar, V., Kansal, S.K., Mehta, S.K.: Toxicity of nanomaterials: present scenario and future scope. In: Islam, N. (ed.) Nanotechnology: recent trends, emerging issues and future directions, pp. 461–486. Nova Science Publishers, New York (2014)
22. Mukherjee, A., Pokhrel, S., Bandyopadhyay, S., Madler, L., Peralta-Videa, J.R., Gardea-Torresdey, J.L.: A soil mediated phyto-toxicological study of iron doped zinc oxide nanoparticles (Fe@ZnO) in green peas (*Pisum sativum* L.). Chem. Eng. J. **258**, 394–401 (2014)
23. Clark, J.H.: Green chemistry: challenges and opportunities. Green. Chem. **1**, 1–8 (1999)
24. Takeuchi, E.S., Murray, R.W.: Metalloporphyrin containing carbon paste electrodes. J. Electroanal. Chem. **188**, 49–57 (1985)
25. Soderberg, J.N., Co, A.C., Sirk, A.H.C., Birss, V.I.: Impact of porous electrode properties on the electrochemical transfer coefficient. J. Phys. Chem. B. **110**, 10401–10410 (2006)
26. Nicholson, R.S., Shain, I.: Theory of stationary electrode polarography single scan and cyclic methods applied to reversible, irreversible, and kinetic systems. Anal. Chem. **36**, 706–723 (1964)
27. Kumar, V., Yadav, S.K.: Plant-mediated synthesis of silver and gold nanoparticles and their applications. J. Chem. Technol. Biotechnol. **84**, 151–157 (2009)
28. Kumar, V., Yadav, S.K.: Influence of physiochemical factors on size of gold nanoparticles synthesised using leaf extract of *Syzygium cumini* L. J. Chem. Sci. Technol. **2**, 104–113 (2013)
29. Mason, C., Vivekanandhan, S., Misra, M., Mohanty, A.K.: Switchgrass *(Panicum virgatum*) extract mediated green synthesis of silver nanoparticles. World J. Nano. Sci. Eng. **2**, 47–52 (2012)
30. Kumar, V., Yadav, S.K.: Synthesis of different-sized silver nanoparticles by simply varying reaction conditions with leaf extracts of *Bauhinia variegata* L. IET Nanobiotechnol. **6**, 1–8 (2012)
31. Halkes, K.M., De Souza, A.C., Maljaars, C.E.P., Gerwig, G.J., Kamerling, J.P.: A facile method for the preparation of gold glyconanoparticles from free oligosaccharides and their applicability in carbohydrate-protein interaction studies. Eur. J. Org. Chem. **2005**, 3650–3659 (2005)
32. Hussain, I., Wang, Z., Cooper, A.I., Brust, M.: Formation of spherical nanostructures by the controlled aggregation of gold colloids. Langmuir **22**, 2938–2941 (2006)
33. Kumar, V., Yadav, S.K.: Synthesis of stable, polyshaped silver and gold nanoparticles using leaf extract of *Lonicera japonica* L. Int. J. Green Nanotechnol. **3**, 281–291 (2011)
34. Khalafi-Nezhad, A., Panah, F.: Size-controlled synthesis of palladium nanoparticles on a silica-cyclodextrin substrate: a novel palladium catalyst system for the heck reaction in water. ACS. Sustain. Chem. Eng. **2**, 1177–1186 (2014)
35. Stobbe, E.R., de Boer, B.A., Geus, J.W.: The reduction and oxidation behavior of manganese oxides. Catal. Today. **47**, 161–167 (1999)
36. Chertihin, G.V., Andrews, L.: Reactions of laser-ablated manganese atoms with dioxygen. Infrared spectra of MnO, OMnO, $Mn(O_2)$, $(MnO)_2$, and higher oxide complexes in solid argon. J. Phys. Chem. A **101**, 8547–8553 (1997)
37. Zhang, Q., Luo, J., Vileno, E., Suib, S.L.: Synthesis of cryptomelane-type manganese oxides by microwave heating. Chem. Mater. **9**, 2090–2095 (1997)
38. Yang, X., Makita, Y., Liu, Z.H., Sakane, K., Ooi, K.: Structural characterization of self-assembled MnO_2 nanosheets from birnessite manganese oxide single crystals. Chem. Mater. **16**, 5581–5588 (2004)
39. Kang, L., Zhang, M., Liu, Z.H., Ooi, K.: IR spectra of manganese oxides with either layered or tunnel structures. Spectrochim. Acta. A. **67**, 864–869 (2007)
40. Maliyekkal, S.M., Lisha, K.P., Pradeep, T.: A novel cellulose-manganese oxide hybrid material by in situ soft chemical synthesis and its application for the removal of Pb(II) from water. J. Hazard. Mater. **181**, 986–995 (2010)
41. Singh, A.K., Talat, M., Singh, D.P., Srivastava, O.N.: Biosynthesis of gold and silver nanoparticles by natural precursor clove and their functionalization with amine group. J. Nanopart. Res. **12**, 1667–1675 (2010)
42. Al-Zier, A., Allaham, H., Latifi, K., Allaf, A.W.: FTIR spectroscopic efficiency of eugenol methylether additive as free radical scavenger agent to sunflower cooking oil at high temperature and different concentrations. Rev. Roum. Chim. **59**, 9–14 (2014)
43. Chowdhry, B.Z., Ryall, J.P., Dines, T.J., Mendham, A.P.: Infrared and raman spectroscopy of eugenol, isoeugenol, and methyl eugenol: conformational analysis and vibrational assignments from density functional theory calculations of the anharmonic fundamentals. J. Phys. Chem. A. **119**, 11280–11292 (2015)
44. Yaghoubian, H., Karimi-Maleh, H., Khalilzadeh, M.A., Karimi, F.: Electrochemical detection of carbidopa using a ferrocene modified carbon nanotube paste electrode. J. Serb. Chem. Soc. **74**, 1443–1453 (2009)
45. Yogeswaran, U., Chen, S.M.: A review on the electrochemical sensors and biosensors composed of nanowires as sensing material. Sensors **8**, 290–313 (2008)
46. Ndlovu, T., Arotiba, O.A., Krause, R.W., Mamba, B.B.: Electrochemical detection of o-nitrophenol on a poly(propyleneimine)-gold nanocomposite modified glassy carbon electrode. Int. J. Electrochem. Sci. **5**, 1179–1186 (2010)